PCCP

Accepted Manuscript

ROYAL SOCIETY OF CHEMISTRY

www.rsc.org/pccp

Physical Chemistry Chemical Physics

PCCP

ARTICLE

A hybrid density functional theory study of the anion distribution and applied electronic properties of the $LaTiO_2N$ semiconductor photocatalyst

Received 00th January 20xx,
Accepted 00th January 20xx

DOI: 10.1039/x0xx00000x

www.rsc.org/

Xin Wang,[a] *Zhaosheng Li*[b] and *Zhigang Zou*[c]

Although the crystallographic space group has been determined, detailed first principles calculations of the $LaTiO_2N$ semiconductor photocatalyst crystal have not been performed because of the nitrogen/oxygen sosoloid-like anion distribution. In this study, based on the Heyd–Scuseria–Ernzerhof method and experimental anion content, we present the possibility of determining detailed information about the $LaTiO_2N$ sosoloid-like anion distribution by dividing the anions into possible primitive cells. The detailed information about the anion distribution based on the characteristics of the energetically acceptable primitive cell structures suggests that the $LaTiO_2N$ structure is composed of aperiodic stacks of six building-block primitive cells, the non-vacancy primitive cells are located at the surface as effective photoreaction sites, and vacancy structures are located in the bulk. The surface oxide-rich structures increase the near-surface conduction band minimum rise and strengthen photoelectron transport to the bulk, while the content of the bulk vacancy structures should be balanced because of being out of photoreactions. This study is expected to provide a different perspective to understanding the $LaTiO_2N$ sosoloid-like anion distribution.

Introduction

Solar hydrogen production by photocatalytic (or photoelectrochemical) water splitting is an effective approach to ease the current energy crisis and prevent environmental problems associated with fossil fuels.[1–4] Much effort has been made to develop stable, reliable, and efficient metal oxide photocatalysts with a visible-light response. Unfortunately, the band gaps of most metal oxides are too large to absorb abundant visible light.

Recently, nitrides and oxynitrides have emerged as promising candidates for water splitting. Among these compounds, perovskite $LaTiO_2N$, with a band gap of 2.1 eV, has recently attracted considerable interest,[5–8] because it is able to absorb abundant visible light of $\lambda \leq 600$ nm and has a theoretical solar-to-hydrogen efficiency of ca. 15.4%.[5] Recently, our group reported a record plateau photocurrent of 6.5 mA/cm^2 on $LaTiO_2N$ photoanodes (AM 1.5 G), which is about half of its theoretical maximum photocurrent (12.5 mA/cm^2).[9] Although $LaTiO_2N$ is promising in the field of the photocatalytic or photoelectrochemical water splitting, some problems associated with $LaTiO_2N$ remain unanswered. To our knowledge, differing from experimental studies, theoretical studies, such as density functional theory (DFT) studies, of $LaTiO_2N$ are very limited.[10,11] A proper explanation of this discrepancy is the difficulty of structure construction in $LaTiO_2N$ theoretical studies. For $LaTiO_2N$, the nitrogen and oxygen atoms are randomly distributed in the anion lattice sites, leading to difficulty in building an exact model of $LaTiO_2N$ for theoretical calculations.[12–14] Therefore, to obtain an in-depth understanding of the physical and chemical properties of $LaTiO_2N$, it is first necessary to clarify the anion distribution of $LaTiO_2N$.

Generally, similar atoms in multiple atom compounds, particularly oxygen and nitrogen in oxynitrides, form solid solutions. An unwarranted preset concept of a sosoloid crystal structure is that there must be a unique supercell structure with fixed atom occupation that is lower in energy than other possible structures. Unfortunately, owe to the formidable calculation, most of the trying to figure out the unique stable supercell structure are failed. Besides, some research indicates that, not all the sosoloid crystal obtains a unique stable supercell structures. Take $LaTiO_2N$, as shown in Figure 1, as an example.[12,14] The anions are located at the six vertices of the Ti-center perovskite octahedron, and anion site 2 and site 3 have equivalent space occupations. Irrespective of what type of supercell structure is built, site 2 and site 3 should achieve the same oxygen and nitrogen occupations as the supercell structure does not change the symmetry of the crystal lattice. Unfortunately, neutron diffraction data suggest that the two sites have different anion occupations (*e.g.*, oxygen content 0.67/0.6 and 0.72/0.52 at site 2/3),[12,14] which means that the size-changing of the supercell structure models could not meet the requirement of the nonuniform anion distribution. In other words, the anion distribution is random and the anions of the whole crystal show aperiodicity, which means that there might not be a definite common supercell structure for $LaTiO_2N$.

*Corresponding author: Zhaosheng Li
E-mail address: zsli@nju.edu.cn

However, because the anions are located at three sites of the Ti-center perovskite octahedrons, each of the perovskite octahedron is a primitive cell in terms of the crystalline space group. The disordered anion distributions could then be transformed into the distribution of denumerable Ti-center perovskite octahedrons with different anion occupations, equivalent to the distributions of the corresponding primitive cell structures. Although the exact periodic superstructure of $LaTiO_2N$ is still unclear, some details about the crystal can be obtained from the properties of the different primitive cell structures. For example, if all of the oxygen-rich primitive cell structures in the $LaTiO_2N$ crystal have the lowest surface energies, then these primitive cell structures should be in the surface layers rather than in the bulk, and the surface layers are oxygen-rich. Therefore, to obtain the properties of a homogeneous $LaTiO_2N$ crystal with the acceptable primitive cell structures, the acceptable structures from all of the possible structures should be first determined using two conditions. (1) The energies of the acceptable structures are generally as low as possible. We will compare their formation energies based on accurate hybrid-DFT calculations. (2) The acceptable primitive cell structures should satisfy the experimental N/O atomic ratio condition. Experiments by Clarke *et al*.[12] revealed that although the nitrogen and oxygen atoms are randomly distributed in the anion lattice sites in $LaTiO_2N$, the N/O atomic ratio in each anion lattice site is constant. Structures that simultaneously meet these two conditions are theoretically acceptable anion distributed primitive cell structures of $LaTiO_2N$. More details about the above two conditions will be discussed in Section 2.

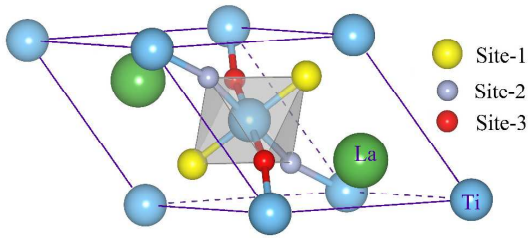

Figure 1. Primitive cell of $LaTiO_2N$: triclinic crystal system with a lattice constant of 5.57 Å and three anion sites (sites 1, 2, and 3) located at the six vertices of the Ti–anion octahedron.

2. Computational details

2.1 Formation energy calculations

As mentioned above, the energies of the acceptable primitive cell structures should be as low as possible. In this study, the formation energies rather than the chemical potentials were used to compare the relative stabilities of the primitive cell structures because the chemical potential confuse the anion content extrema. The formation energy of the $LaTiO_2N$ primitive cell structure is defined as[15,16]

$$\Delta E^f_{Struct} = E^t_{Struct} - E^t_{Stable} - \sum_{i=N,O} (n^i_{Struct} - n^i_{Stable}) E_i \qquad (1)$$

where E^t_{Struct} is the total energy of the a primitive cell structure, E^t_{Stable} is the total energy of the reference primitive cell structure, E_i is the energy per atom of the dimer or the elementary substance of the subscript, and n^i_{Struct} and n^i_{Stable} are the number of anions in the corresponding bulk structure.[17] According to Eq. (1), a negative energy means a stable structure. The pyrolysis temperature of a crystal indicates that the crystal is in the finite temperature well from a minimum temperature of absolute zero to a maximum temperature of the pyrolysis temperature (see Figure S1 in the ESI†). Therefore, although a stable structure theoretically means a structure with a low formation energy in the ground state, the primitive cell structures within the well depth to the reference stable structures should be the same stability to the reference structure. The temperature well could be simplified to an energy well, and the corresponding energy is directly proportional to the temperature with the Boltzmann constant.[18] As a result, the thermal energy depth of the well should be 0.1 eV for $LaTiO_2N$, which corresponds to the pyrolysis temperature 1240–1300 K.[8,19] If the formation energy of a primitive cell structure is less than 0.1 eV from a stable structure, the structure should be considered as stable.

Randomly placing the O and N atoms on $LaTiO_2N$ anion site1, 2, and 3, there are 27 primitive cell structures without vacancies (see Table S1 in ESI†). The acceptable anion distributions of the primitive cell structures should be among the 27 structures together with their anion vacancy structures. The energies of the 27 structures and their vacancy structures were obtained by DFT calculations using the VASP code[20,21] together with the Heyd–Scuseria–Ernzerhof (HSE) method.[22,23] The two parameters for the HSE calculation were α = 0.25 and ω = 0.2 $Å^{-1}$, which refers to the HSE06 functional.[24–26] The cutoff energy was 420 eV and the Brillouin zone integration was 3×3×3 *k*-point meshes. The geometry optimizations were performed until the residual forces on each ion were less than 0.02 eV/Å. Supercell testing calculations were applied and the primitive cell model was sufficient to obtain reliable results.

2.2 Anion ratio condition

As shown in Figure 1,[12,14] one Ti–anion (anion = N or O) octahedron is located at the center of the $LaTiO_2N$ primitive cell, resulting in three independent anion sites (site1, 2, and 3). As discussed in Section 1, experiments by Clarke *et al*.[12,14,27,28] revealed that the oxygen contents of the three anion sites are fixed and different (*e.g.*, 0.72/0.67/0.6 at site1/2/3[12]). As a result, the fixed oxide fractions at the three anion sites provide the second condition that acceptable primitive cell structures should satisfy. Considering the 27 primitive cell structures and their anion vacancy structures, the oxide fractions at the three sites can be expressed as

$$\varphi_j = \frac{\sum_k (1-\phi_{kj}) n^O_{k,j} X_k}{\sum_k (2-\phi_{kj} n^O_{k,j} - \Phi_{kj} n^N_{k,j}) X_k}, k = 1,2,3... \qquad (2)$$

where *k* is the number of the primitive cell structure, X_k is the percentage of structure *k* in a crystalline grain (obviously, $\sum_k X_k = 1$), $n^O_{k,j} / n^N_{k,j}$ are the number of O/N atoms at site *j* of structure *k*, and ϕ_{kj} / Φ_{kj} is the O/N vacancy rate of structure *k* at site *j*. The numerator denotes the number of oxygen atoms in ideal monocrystalline $LaTiO_2N$, while the denominator

denotes the total number of anions. The ratio of the numerator to the denominator is then the fraction of oxygen atoms at site *j*. The total oxide fraction in an ideal monocrystalline $LaTiO_2N$ is

$$\frac{\sum_{j=1}^{3}\sum_{k}(1-\phi_{kj})n_{k,j}^{O}X_k}{\sum_{j=1}^{3}\sum_{k}(2-\phi_{kj}n_{k,j}^{O}-\Phi_{kj}n_{k,j}^{N})X_k}=\varphi_{tol} \quad (3)$$

where *j* is the site number (1, 2, or 3). The numerator similarly denotes the sum of oxygen atoms at all three sites in an ideal $LaTiO_2N$ infinite monocrystalline crystal, while the denominator denotes the sum of the anion numbers. The ratio of the numerator to the denominator is then the total fraction of oxygen atoms in the crystal. As mentioned above, the oxygen contents at the three anion sites are different.[12,14] The total oxygen contents of different $LaTiO_2N$ samples[5–7,12,14,29] show that the oxide component is higher than the charge balance requirement. Therefore, the total oxide fraction should vary with changes of the intrinsic crystal conditions (*e.g.*, crystallinity, grain size, and surface structures). If the group of anion-distributed primitive cell structures matches the N/O atomic ratio conditions, Eqs. (2) and (3) give general solutions rather than particular solutions.

3. Results and discussion

3.1 Crystal structures

The possible primitive cell structures can be divided into two groups: the 27 N/O randomly occupied structures and their anion vacancy structures. Because the $LaTiO_2N$ crystal is supposed to be an ideal charge balance structure, it is meaningful to take the charge balance primitive cell structures as the reference stable structures because their energies are lower than the other structures (see Figure 2). As shown in Figure 2(a), the formation energies of structures M_2 and M_3 are 0.06 eV lower than M_1, while those of M_4, M_5, and M_6 are 0.32 eV higher than M_1. Therefore, M_1, M_2, and M_3 should be considered as acceptable primitive cell structures because their formation energy are less than 0.1 eV from the lowest energy structure (Figure S1 in ESI†). Anion ratio calculations of M_1, M_2, and M_3 with Eqs. (2) and (3) indicate that there are no general solutions but particular solutions for M_1, M_2, and M_3, and there might be primitive cell structures among M_7–M_{27}. The formation energies of the oxygen-rich primitive cell structures (*i.e.*, M_7–M_{10}) and nitrogen-rich primitive cell structures (*i.e.*, M_{11}–M_{27}) are shown in Figure 2(b) and (c), respectively. Among the 21 primitive cell structures M_7–M_{27}, only M_8 and M_9 should be considered acceptable structures because their formation energies are less than 0.1 eV from that of the lowest energy structure (*i.e.*, M_8). Unfortunately, the anion ratios of the low energy structures M_1, M_2, M_3, M_8, and M_9 calculated using Eqs. (2) and (3) have no general solutions but particular solutions. Therefore, the non-vacancy structures are not a complete group of acceptable primitive cell structures for the $LaTiO_2N$ anion distributions, and anion vacancies exist in $LaTiO_2N$.

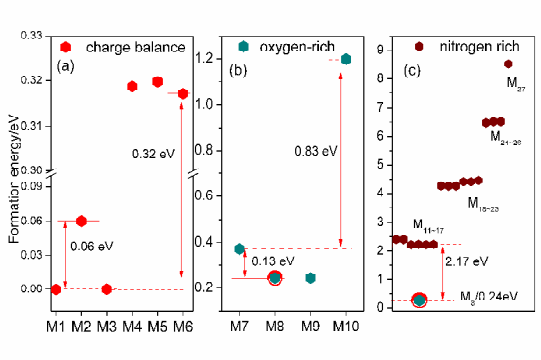

Figure 2. Formation energies of the bulk structures of (a) M_1–M_6, (b) M_7–M_{10}, and (c) M_{11}–M_{27} with respect to the formation energy of M_1.

Because there are anion vacancies in $LaTiO_2N$, we further investigated the 27 primitive cell structures with anion vacancies. Note that the $LaTiO_2N$ crystal is taken as homogeneous. The N/O ratio Eq. (2) for M_{11}–M_{27} together with the non-vacancy structures gives no general solutions to satisfy the oxygen content difference at sites 1, 2, and 3 and the total oxygen-rich content, and the vacancy structures M_{11}–M_{27} should be out of acceptable structures. There is both trivalent and tetravalent titanium in $LaTiO_2N$,[30,31] and thus there is a charge balance limit for the anion distribution, especially for the anion vacancies. However, the anion vacancy numbers, namely *x* and *y* in the primitive cell structural formula $La_2Ti_2O_{4+\Delta-x}N_{2-\Delta-y}$ (where Δ is the weighting factor for the O/N ratios of the non-vacancy structures), have no values greater than 1 to obtain a total oxygen-rich content (*i.e.*, higher than 0.667).[5–7] Furthermore, the anion distribution was taken as fully developed and homogeneous in the physical DFT calculation size, because divacancy structures could not coexist with non-vacancy structures in a small homogeneous lattice, and the anion vacancy should be monovacant rather than divacant or greater vacancy. Accordingly, there are 39 different anion vacancy structures for M_1–M_{10}, and the formation energies of the 15 vacancy structures of M_1–M_3, 9 of M_4–M_6, and 15 of M_7–M_{10} are shown in Figure 3. Only five oxygen vacancy structures (M_1 at site 3, M_2 at site 1, 2, and 3, and M_3 at site 2 in Figure 4(a)) have vacancy energies less than 0.1 eV from the lowest energy structure (*i.e.*, M_2 at site 1). Thus, the low energy vacancy structures should be M_1/site 3, M_2/site 1, 2, and 3, and M_3/site 2.

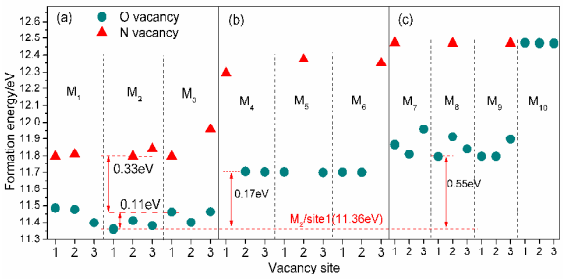

Figure 3. Formation energies of anion vacancy structures with respect to the formation energy of M_1: (a) M_1–M_3, (b) M_4–M_6, and (c) M_7–M_{10}. The reference vacancy structure is the lowest vacancy energy of all of the structures (*i.e.*, an oxygen vacancy of M_2 at site 1).

After the formation energy analysis of all the possible primitive cell structures in $LaTiO_2N$, we found that $LaTiO_2N$ should be composed of five non-vacancy structures (M_1–M_3, M_8, and M_9) and five vacancy structures (M_1/site 3, M_2/site 1, 2, and 3, and M_3/site 2). The Ti–anion octahedral structures of these primitive cell structures are shown in Figure 4. To simplify the N/O atomic ratio equations, the primitive cell content of each vacancy structure is transformed into the vacancy rate at the three sites (namely, ϕ_{kj} / Φ_{kj} in Eqs. (2) and (3)). Obviously, the vacancy rates of each site should be less than 100%

$$\phi_{kj} n^k_{O,j} < 1, \forall(\mathrm{k,j}) \in ([1,2,3,8,9],[1,2,3]) \quad (4)$$

In addition, the positive charge deviation is limited within Ti^{4+} to Ti^{3+}, and then the corresponding anion charge deviation should satisfy

$$\sum_{k=1,2,3,8,9} \sum_{j=1}^{3} (\frac{1}{2} \mathrm{n}^k_{N,j} X_k - \phi_{kj} n^k_{O,j} X_k) \in (0,1) \quad (5)$$

The details of the oxide vacancy rate matrix $\Phi_{\mathrm{k,j}}$ for M_1–M_3, M_8, and M_9, and solutions of the anion ratio equations for vacancies in M_1–M_3, M_8, and M_9 are shown in Section 4 of the ESI†. The percentage of M_1 is much smaller than the other four structures, suggesting that both M_1 with/without vacancies should be excluded (Figure S4 in ESI†). The values of the vacancy rates (Figure S5 in ESI†) reveal that vacancies in M_2 at site 1 and 2 should be excluded, whereas the vacancies in M_2 at site 3 and M_3 at site 2 must be included in $LaTiO_2N$. Therefore, we finally found that the acceptable primitive cell group of $LaTiO_2N$ contains the four non-vacancy structures M_2, M_3, M_8, and M_9 and the two anion-vacancy structures M_2/site 3 and M_3/site 2.

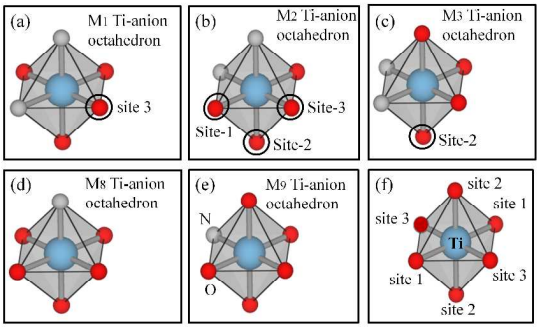

Figure 4. Ti-center octahedrons of stable structures M_1–M_3, M_8, and M_9 with the five oxygen vacancy positions marked with black circles. (a) Ti–anion octahedron of M_1 with the vacancy at site 3. (b) M_2 with vacancies at site 1, 2, and 3. (c) M_3 with a vacancy at site 2. (d) M_8 and (e) M_9. The Ti–La lattices and sites are shown in (f), as same as that in Figure 1.

3.2 Electronic properties

Further calculations of the junctions between the acceptable structures (Figure S6 in ESI†) indicates that the binding energies of the junctions are much higher than those of each pure structure. Therefore, the primitive cells of each structure will self-aggregate rather than being randomly distributed in the crystal. Furthermore, the tendency of the calculated surface energies of the three representative crystal surfaces ((001), (010), and (001)) are consistent. Taking the (001) surface (Figure 5(a)) as an example, the non-vacancy primitive cells (M_2, M_3, M_8, and M_9) have low surface energies and will be surface layers while the vacancy primitive cells will exist in the bulk. As a result, the proposed structure of the $LaTiO_2N$ crystal is shown in Figure 5(b). The non-vacancy primitive cells (*i.e.*, M_2, M_3, M_8, and M_9) will gather together in the surface layers as $LaTiO_2N$ photoreaction sites while the vacancy structures exist in the bulk (M_2/M_3 vacancy at site 3/2).

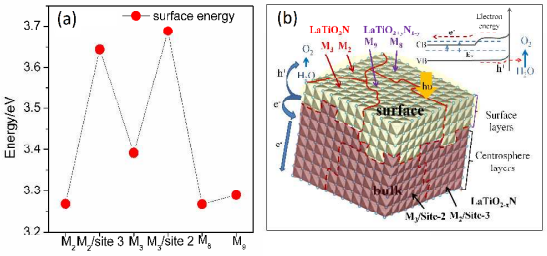

Figure 5. (a) Surface energies of M_2, M_3, M_8, and M_9, and M_2/M_3 with a vacancy at site 3/2. (b) Diagrammatic cross-section of the proposed $LaTiO_2N$ grain. The non-vacancy primitive cells are located at the surface while the vacancy primitive cells are located in the bulk.

The DOS structures of M_2, M_3, M_8, and M_9, and the vacancy structures M_2/M_3 at site 3/2 are shown in Figure 6. The distances between the valence band maximum (VBM) and conduction band minimum (CBM), the calculated minimum band gap (E_g), are 2.21/2.14 eV for M_2/M_3, which are consistent with experimental measurements (2.1–2.3 eV for $LaTiO_2N$[8,11,32]), while E_g = 2.82 eV for the charge stable M_8 and M_9 structures. Furthermore, M_2, M_3, M_8, and M_9 have the same Fermi level (the primitive cells are in a single crystal) and the same VBM (see Figure 6). Therefore, the junctions of M_2/M_3 and M_8/M_9 in the surface layers will have a CBM increase (see Figure 5(b)). The near-surface layer CBM increase will result in an electronic chemical potential decrease and flatband potential decrease,[33] leading to strengthened transport for the surface photoinduced electrons to the bulk. The DOS of the vacancy structures (M_2/M_3 at site 3/2) shows that the Fermi energy levels (E_F) across the CB level and the vacancy structures achieve high conductivity, and thus the transport for photoinduced electrons in the surface layers to the bulk will be further strengthened. In general, the photoreaction occurs on the non-vacancy structures in the surface layers of $LaTiO_2N$. The surface oxide-rich structures lead to the CB level increase, the flatband potential decrease, and strengthening of the photoinduced electron transport to the bulk, while the bulk vacancy structures provide good

conductivity and further strengthen electron transport. Although the vacancy structures supply a much better electronic transport process than the oxide-rich structures, their content should be balanced because their existence leads to a decrease of the content of the effective photoreaction structures M_2, M_3, M_8, and M_9 (more than a 25% decrease, as shown in Figure S4(a) in the ESI†).

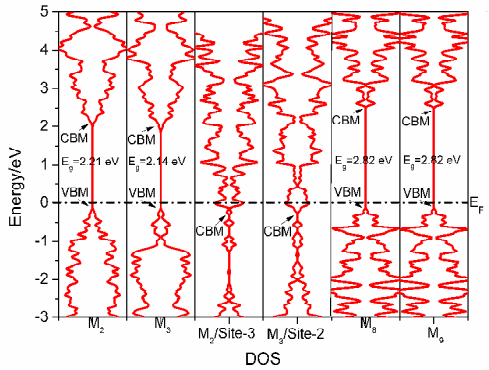

Figure 6. DOS structures of M_2 and M_3, charged M_8 and M_9, and M_2/M_3 with a vacancy at site 3/2. The horizontal line is the Fermi level (*i.e.*, the energy zero).

Conclusions

In this study, the anion distributions of the $LaTiO_2N$ semiconductor photocatalyst were investigated by hybrid-DFT calculations. The disordered sosoloid-like anion distributions transformed to the distribution of several particular acceptable primitive cell structures from all the possible primitive cell structures of $LaTiO_2N$. Based on the character of the primitive cell structures, the proposed $LaTiO_2N$ structure is composed of a stack of six building-block primitive cells with the same titanium lattice but different perovskite anion octahedron. The surface non-vacancy structures are effective photoreaction sites and the oxide-rich surface leads to a near-surface CBM increase together with better photoinduced electron transport from the surface to the bulk. The bulk vacancy structures strengthen the surface electron transport, but their content should be balanced because they are not involved the photoreactions. Although further work should be performed to investigate the detailed statistical properties of the primitive cells and the whole crystal, we hope that these results are helpful in the investigation of the $LaTiO_2N$ oxynitride semiconductor photocatalyst.

Acknowledgements

This work was supported by the National Basic Research Program of China (2013CB632404).

Notes and references

National Laboratory of Solid State Microstructures, Department of Physics, Ecomaterials and Renewable Energy Research Center (ERERC), and College of Engineering and Applied Sciences, Nanjing University, 22 Hankou Road, Nanjing 210093, People's Republic of China.

*Corresponding Authors:
E-mail: zsli@nju.edu.cn

†
Electronic Supplementary Information (ESI) available:[]

1. M. Grätzel, *Nature*, 2001, **414**, 338-344.
2. N. S. Lewis and D. G. Nocera, *Proceedings of the National Academy of Sciences*, 2006, **103**, 15729-15735.
3. O. Khaselev and J. A. Turner, *Science*, 1998, **280**, 425-427.
4. A. Fujishima and K. Honda, *Nature*, 1972, **238**, 37-38.
5. A. Kasahara, K. Nukumizu, G. Hitoki, T. Takata, J. N. Kondo, M. Hara, H. Kobayashi and K. Domen, *The Journal of Physical Chemistry A*, 2002, **106**, 6750-6753.
6. D. Fasquelle, A. Ziani, C. Le Paven-Thivet, L. Le Gendre and J. Carru, *Materials Letters*, 2011, **65**, 3102-3104.
7. C. M. Leroy, A. E. Maegli, K. Sivula, T. Hisatomi, N. Xanthopoulos, E. H. Otal, S. Yoon, A. Weidenkaff, R. Sanjines and M. Gratzel, *Chemical communications*, 2012, **48**, 820-822.
8. D. Logvinovich, A. Börger, M. Döbeli, S. G. Ebbinghaus, A. Reller and A. Weidenkaff, *Progress in Solid State Chemistry*, 2007, **35**, 281-290.
9. J. Y. Feng, W. J. Luo, T. Fang, H. Lv, Z. Q. Wang, J. Gao, W. M. Liu, T. Yu, Z. S. Li and Z. G. Zou, *Advanced Functional Materials*, 2014, **24**, 3535-3542.
10. A. Kasahara, K. Nukumizu, T. Takata, J. N. Kondo, M. Hara, H. Kobayashi and K. Domen, *Journal of Physical Chemistry B*, 2003, **107**, 791-797.
11. T. Moriga, D. Aoki, Y. Nishida, K. Kitaji, K. Takahara, K.-i. Murai and I. Nakabayashi, *physica status solidi (a)*, 2006, **203**, 2818-2822.
12. S. J. Clarke, B. P. Guinot, C. W. Michie, M. J. C. Calmont and M. J. Rosseinsky, *Chem. Mat.*, 2002, **14**, 288-294.
13. M. Yashima, M. Saito, H. Nakano, T. Takata, K. Ogisu and K. Domen, *Chem. Commun.*, 2010, **46**, 4704-4706.
14. D. Logvinovich, L. Bocher, D. Sheptyakov, R. Figi, S. G. Ebbinghaus, R. Aguiar, M. H. Aguirre, A. Reller and A. Weidenkaff, *Solid State Sciences*, 2009, **11**, 1513-1519.
15. M. Gillan, *Journal of Physics: Condensed Matter*, 1989, **1**, 689.
16. S. Zhang and J. E. Northrup, *Physical review letters*, 1991, **67**, 2339.
17. A. Zoroddu, F. Bernardini, P. Ruggerone and V. Fiorentini, *Phys. Rev. B*, 2001, **64**, 045208.
18. T.-D. Lee, *Shanghai Scientific and Technical Publishers*, 2006.
19. D. Li, W. Li, C. Fasel, J. Shen and R. Riedel, *Journal of Alloys and Compounds*, 2014, **586**, 567-573.
20. G. Kresse and J. Hafner, *Phys. Rev. B*, 1993, **47**, 558.
21. G. Kresse and J. Furthmüller, *Computational Materials Science*, 1996, **6**, 15-50.
22. T. M. Henderson, J. Paier and G. E. Scuseria, *Phys. Status Solidi B-Basic Solid State Phys.*, 2011, **248**, 767-774.
23. J. Paier, R. Asahi, A. Nagoya and G. Kresse, *Phys. Rev. B*, 2009, **79**.
24. M. V. Ganduglia-Pirovano, J. L. F. Da Silva and J. Sauer, *Physical Review Letters*, 2009, **102**.
25. P. G. Moses and C. G. Van de Walle, *Appl. Phys. Lett.*, 2010, **96**.
26. J. P. Perdew, M. Emzerhof and K. Burke, *J. Chem. Phys.*, 1996, **105**, 9982-9985.
27. M. Yashima, M. Saito, H. Nakano, T. Takata, K. Ogisu and K. Domen, *Chemical communications*, 2010, **46**, 4704-4706.

28. D. Logvinovich, S. G. Ebbinghaus, A. Reller, I. Marozau, D. Ferri and A. Weidenkaff, *Zeitschrift für anorganische und allgemeine Chemie*, 2010, **636**, 905-912.
29. A. E. Maegli, S. Pokrant, T. Hisatomi, M. Trottmann, K. Domen and A. Weidenkaff, *The Journal of Physical Chemistry C*, 2013, 131118072322003.
30. F. Lichtenberg, D. Widmer, J. G. Bednorz, T. Williams and A. Reller, *Z. Phys. B-Condens. Mat.*, 1991, **82**, 211-216.
31. M. Matsukawa, R. Ishikawa, T. Hisatomi, Y. Moriya, N. Shibata, J. Kubota, Y. Ikuhara and K. Domen, *Nano Lett*, 2014, **14**, 1038-1041.
32. A. E. Maegli, E. H. Otal, T. Hisatomi, S. Yoon, C. M. Leroy, N. Schauble, Y. Lu, M. Gratzel and A. Weidenkaff, *Emrs Symposium T: Materials for Solar Hydrogen Via Photo-Electrochemical Production*, 2012, **22**, 61-66.
33. J. Bisquert, P. Cendula, L. Bertoluzzi and S. Gimenez, *The Journal of Physical Chemistry Letters*, 2013, **5**, 205-207.